Article

Zinc as a Promising Anodic Material for All-Solid-State Lithium-Ion Batteries

Kishore Singh [1], Yuchen Yao [2], Takayuki Ichikawa [2], Ankur Jain [1,3,*] and Rini Singh [2,*]

1 Centre for Renewable Energy & Storage, Suresh Gyan Vihar University, Jaipur 302017, India
2 Graduate School of Advanced Science and Engineering, Hiroshima University, Higashi-Hiroshima 739-8527, Japan
3 Natural Science Center for Basic Research & Development, Hiroshima University, Higashi-Hiroshima 739-8530, Japan
* Correspondence: ankur.j.ankur@gmail.com (A.J.); rini@hiroshima-u.ac.jp (R.S.)

Abstract: Electrochemical energy storage is considered a remarkable way to bridge the gap between demand and supply due to intermittent renewable energy production. All-solid-state batteries are an excellent alternative and are known to be the safest class of batteries. In the present scenario to accomplish the energy demands, high-capacity and stable anodes are warranted and can play a vital role in technology upgradation. Among the variety of anodes, alloying-type anodes are superior due to their high gravimetric capacity and stability. In the present work, zinc metal was implemented as electrode material in an all-solid-state lithium-ion battery. This anode material was tested with two different solid-state electrolytes, i.e., lithium borohydride ($LiBH_4$) and halide-stabilized $LiBH_4$ (i.e., $LiBH_4.LiI$). In a coin cell, Li foil was placed as a counter electrode. The establishment of a reaction mechanism during the charging and discharging was obtained through X-ray diffraction (XRD) and cyclic voltammetry (CV). Systematic studies using the temperature dependence performance were also conducted. The volumetric density with both electrolytes was found at more than 3000 mAh/cm^3. The coulombic efficiency for the electrode material was also observed at ~94%. These impressive numbers present zinc electrodes as a promising material for future electrode material for all-solid-state Li-ion batteries.

Keywords: zinc-based anode; all-solid-state; electrochemical performance; Li-ion battery; $LiBH_4$; $LiBH_4.LiI$

1. Introduction

Fulfilling the dream of a clean environment can be possible by the accomplishment and complete exploitation of renewable sources of energy [1–5]. High-performance energy storage technology is gaining the attention of the research community. Battery technology is being used for a wide range of applications, including powering electrical vehicles, integrating intermittent renewable energy, electric gadgets, etc. The accomplishments of future demands of energy requirement are strenuous by the currently used technology in lithium-ion batteries. Li-ion batteries have several advantages, including long cycle life, high stability, high energy density, and higher working potential [6–10].

At present, Li-ion battery technology is based on flammable liquid electrolytes. It has been observed many times that batteries explode during usage. This is a major concern for application safety. All-solid-state Li-ion batteries (ASSLIBs) are the greatest alternative in this regard [11–15]. ASSLIBs consist of electrodes and electrolytes entirely in solid form. Comparatively, these solids are less prone to fire than conventional liquid electrolytes. In the advancement of ASSLIBs, the search for stable, solid electrolytes is considered a major area of research [16–19]. There are several established electrolytes, including hydrides, sulfides, halides, etc. [20–27]. Among them, $LiBH_4$ is one of the interesting electrolytes that provides higher conductivity compared to sulfide-based electrolytes [28–31]. $LiBH_4$

possesses two different structures, i.e., octahedral below 115 °C and hexagonal higher than 115 °C. This hexagonal phase possesses higher conductivity[30]. Many reports have been published using $LiBH_4$ electrolytes, which provide stability toward different anode materials [32–34]. This electrolyte has many advantages; however, it cannot be used at a lower temperature than 115 °C due to its poor ionic conductivity. Researchers established that the combination of $LiBH_4$ with halides enhanced the ionic conductivity considerably and, additionally, enabled $LiBH_4$ to perform at room temperature with a stable cycle life [35].

High-capacity and stable electrochemical anode materials are continuously exploited. The current battery technology relies on graphite-based anodes, which have lower theoretical gravimetric capacity and volumetric capacity, i.e., 372 $mAhg^{-1}$ and ca. 840 $mAhcm^3$, respectively. Sufficient efforts to investigate alloying-type anodes have been attempted by researchers due to their higher capacity than graphite-based anodes. The class of these materials includes known systems, such as Li-Bi, Li-Sn, Li-Si, Li-Ge, Li-Sb, etc. [36–38]. These alloying materials have the advantage of reacting with a considerable number of Li ions reversibly. Despite the many advantages of the above alloying materials, the research community cannot deny the fact that they suffer from large volume expansion, which causes hindered cycle life. For example, silicon delivers a capacity of almost 4200 $mAhg^{-1}$ but suffers a volume expansion of almost 400% compared to graphite-based anodes having only 10%.

Zinc (Zn) has been considered as a promising material for various applications, including Li-ion batteries. It is an alloying-type anode material with higher theoretical capacity and volumetric capacity, i.e., 410 $mAhg^{-1}$ and 2970 $mAhcm^3$, respectively [39], which are higher than commercial graphite-based anodes. During alloying with Li ions, a low operating potential has been observed, corresponding to the formation of different intermetallic phases. Adding to these advantages for commercial applications, zinc is a cost-effective, abundant, and environmentally friendly material. This material can be proved as a good alternative to presently used anodes for future technology. However, a detailed explanation of the reaction mechanism of bulk zinc with lithium is lacking for ASSLIBs.

In our recent report, Li-Bi and Li-Sb systems were investigated in detail to establish Bi and Sb as efficient and stable anodes for ASSLIBs [37]. The anodes were tested for their electrochemical performances with $LiBH_4$ as a solid electrolyte and Li foil as a counter electrode at 120 °C. In this work, zinc is implemented as an anode material for ASSLIBs. The multistep alloying mechanism is observed and explained using X-ray diffraction and cyclic voltammetry experiments. Two different solid electrolytes, $LiBH_4$ and $LiBH_4.LiI$, are tested for the cyclic stability of the anodic material. The temperature-dependent (performance at 120 °C, 90 °C, 60 °C, and 30 °C) behavior of the Zn anode with the $LiBH_4.LiI$ electrolyte is investigated.

2. Results and Discussion

Initially, the cells of combination (Zn, $LiBH_4$, and AB)/$LiBH_4$/Li foil were tested. The XRD spectra of the composite anode are shown in Figure 1. Major intense peaks corresponded to the zinc metal. Small peaks corresponding to the electrolyte, i.e., $LiBH_4$, were also visible. The electrochemical behavior of the cell was tested between the range of 0.01–1.5 V at 120 °C. The reason for testing in this range was to avoid the thermochemical reaction of $LiBH_4$ with zinc metal that has been reported for some electrode materials [40,41]. The first discharge and charge capacity of the Zn electrode were found at 507 and 327 $mAhg^{-1}$, respectively, as depicted in Figure 2b. The discharge capacity of the cell was higher than the theoretical capacity of Zn (i.e., LiZn has a capacity of 410 $mAhg^{-1}$). There were two possible reasons for this higher capacity. The first was due to the contribution of carbon (AB), and the second possibility was the formation of a solid solution of Li and Zn. The possibility of solid solution formation was only during electrochemical cycling because, after milling, the separate phases of $LiBH_4$ and Zn appeared in the XRD spectrum. Several plateaus appeared during both the charging and discharging processes.
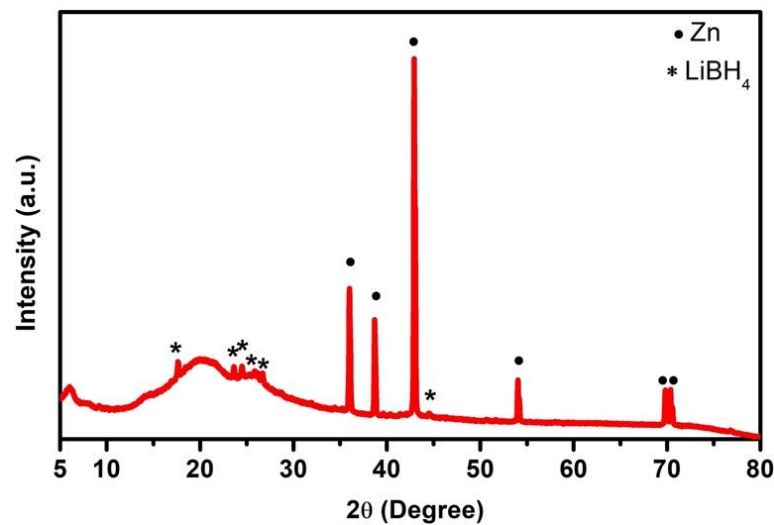
Figure 1. XRD spectrum of Zn-LiBH$_4$-AB composite anode. The JCPDS numbers corresponding to different phases are Zn (00-087-0713) and LiBH$_4$ (00-008-1460).
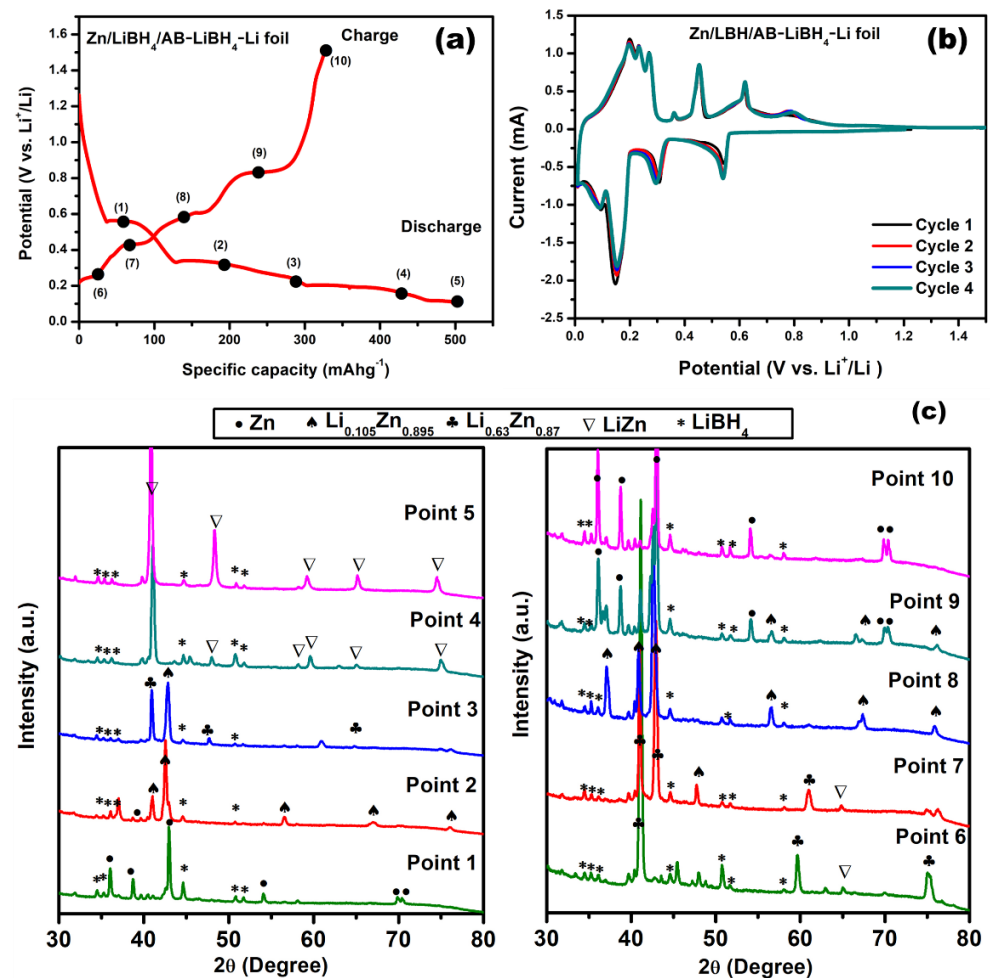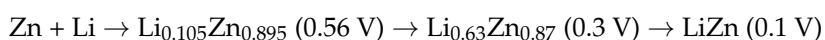

Figure 2. (**a**) First galvanostatic discharge–charge profile for Zn$-$LiBH$_4$$-$AB/LiBH$_4$/Li foil coin cell; (**b**) cyclic voltammetry curves; (**c**) X-ray diffraction profiles of the Zn$-$LiBH$_4$$-$AB/LiBH$_4$/Li foil coin cell at different charge–discharge potentials of first electrochemical discharge–charge process. The JCPDS numbers corresponding to different phases are Zn (00-087-0713), Li$_{0.105}$Zn$_{0.895}$ (00-002-7089), Li$_{0.63}$Zn$_{0.87}$ (00-008-1460), LiZn (00-000-8410), and LiBH$_4$ (00-008-1460).

To further elucidate the reversibility of the reaction, the CV measurements of half cells were taken between the potential range of 0.01–1.5 V (Li^+/Li) with the scan rate of 0.1 mV/s. Complementary to the electrochemical reaction, CV measurements also witnessed several cathodic and anodic peaks (Figure 2a), which were located at almost the same potentials. The reversibility of the reaction was confirmed by the cycling (four cycles) in CV measurements, which showed exactly similar curves.

The potentials of all the CV peaks were matched with the plateau potentials on the charging–discharging curve in Figure 2a very well. Several XRD experiments were conducted by stopping the cells after each plateau in order to comprehend the reaction mechanism. Figure 2a displays the selected potential points as numbers for XRD measurements, and Figure 2c shows the associated XRD profiles. Several phases of LiZn exist according to the phase diagram of Li-Zn[41], which were also observed in the present study. The distinct peaks of the $LiBH_4$ (JCPDS card number 00-008-1460) and Zn phases were seen in the first XRD scan, which was taken at the discharge potential of 0.56 V (point 1, Figure 2a). The peaks corresponding to the Zn phase were still present, but their intensity and position were slightly altered, which was due to the formation of a Li-Zn solid solution. Due to the reduction in peak intensity of the Zn phase, the presence of $LiBH_4$ was also more evident in comparison to the as-prepared composite anode (Figure 1). On further lithiation, at point (2) when the potential was 0.34 V, two distinct phases, namely Zn (JCPDS number-00-087-0713) and $Li_{0.105}Zn_{0.895}$ (JCPDS number-00-002-7089) appeared. Lowering the potential down to 0.21 V caused further lithium insertion into the composite electrode material. Another phase with higher Li content, i.e., $Li_{0.63}Zn_{0.87}$ (JCPDS number-00-008-1460) appeared in addition to the previously formed $Li_{0.105}Zn_{0.895}$ phase. A saturation of Li into Zn was achieved at point 4 (0.13 V) and point 5 (0.1 V), which was evident from the presence of peaks corresponding to the LiZn phase (JCPDS number-00-000-8410). It was note that LiZn was the phase with the highest possible Li content according to the Li-Zn phase diagram [39], which suggests the completion of the lithiation reaction. Similar to discharging, a multistep reaction was seen during the charging process. Several separate peaks of various phases, including LiZn, $Li_{0.63}Zn_{0.87}$, and $LiBH_4$, were present at point 6 (0.27 V) during charging. The $Li_{0.63}Zn_{0.87}$ and $Li_{0.105}Zn_{0.895}$ were seen at potential 0.45 V, which was designated as point 7. The dominant phase, $Li_{0.105}Zn_{0.895}$, emerged at point 8 with a potential of 0.56 V, which was favorable to the discharge outcomes. The peaks corresponding to Zn started appearing at point 9, along with the $Li_{0.105}Zn_{0.895}$ phase. Approaching potential 1.5 V completely charged the cell and only the Zn phase existed, along with $LiBH_4$, which was similar to the as-prepared sample. This confirmed that the reaction was reversible and that all of the plateaus arose when this cell was cycled between 0.1–1.5 V. Since $LiBH_4$ was a component (electrolyte) of the anode composite, its peaks were observed in all the XRD spectra.

Based on the electrochemical, CV, and XRD results, the mechanism could be proposed as below.

During discharge:

$$Zn + Li \rightarrow Li_{0.105}Zn_{0.895} \ (0.56 \ V) \rightarrow Li_{0.63}Zn_{0.87} \ (0.3 \ V) \rightarrow LiZn \ (0.1 \ V)$$

During charging:

$$LiZn \rightarrow Li_{0.63}Zn_{0.87} \ (0.42 \ V) \rightarrow Li_{0.105}Zn_{0.895} \ (0.83 \ V) \rightarrow Zn \ (1.5 \ V)$$

In order to compare and to understand the reaction more clearly, an electrochemical test of pure Zn metal was also performed without the addition of $LiBH_4$ and AB. The electrochemical profile is shown in Supplementary Materials Figure S1. The profile of the pure Zn anode was very different from the composite (reported herein) and the other reports. The first discharge and charge capacities were found around 290 and 140 mAhg^{-1}, respectively. From the second cycle onwards, the capacity was drastically decreased. Different plateaus from the Li–Zn reactions were also not observed. It was concluded from

this result that, without any conductive support (AB) or interface between the electrode and electrolyte ($LiBH_4$), pure Zn electrodes could not work properly. The reaction happened during charging and discharging, and the XRD measurements were performed at each reaction potential. The different plateaus of the electrochemical profile were assigned numbers from 1–10 for a better understanding of the reaction at each point. Numbers from 1–5 were assigned reactions during discharging, and numbers from 6–10 were assigned to the charging. The XRD results are shown in Figure 2c during the discharging of the cell (reference points 1, 2, 3, 4, and 5), while the charging points (reference points 6, 7, 8, 9, and 10) were assigned.

$LiBH_4$ has been proved an excellent solid-state electrolyte in terms of stability and conductivity for various bismuth and antimony chalcogenide materials, metal hydrides, and sulfide-based electrode materials [32,34,37,42]. However, its high conductivity can be realized only at a high temperature (>115 °C) due to structural transition at this temperature. The practical applications demand room-temperature operations of these cells. With this intention, $LiBH_4$ needs to be tuned to achieve high conductivity at ambient temperature. In this context, $LiBH_4.LiI$[43] was found an effective electrolyte for different metal hydrides, so the implementation of this electrolyte was performed in the electrolyte layer, along with $LiBH_4$, for the cell comparison. To explore the performance of this cell, the charging–discharging experiments were performed at different temperatures, i.e., 120 °C, 90 °C, 60 °C, and 30 °C (Figure 3a). The current rate for these cells was kept constant, i.e., at 0.1 C. The capacity at 120 °C was observed as 583 $mAhg^{-1}$, which was even higher than the cell having $LiBH_4$ in the electrolyte layer (Figure 2a). The capacity values were obtained as 531, 427, and 175 $mAhg^{-1}$ at 90 °C, 60 °C, and 30 °C, respectively. By reducing the temperature, the capacity of the cells was found to be lower, while the electrochemical plateaus were observed at almost similar potentials for the different temperatures. The reasons for this behavior were reduced diffusivity and increased electrical polarization at lower temperatures. On the other hand, the cell with $LiBH_4$ in the electrolyte layer did not work at all the lower temperatures. To explore the capability of the prepared electrode, along with the $LiBH_4$-LiI, the cyclic stability of the electrode using both electrolytes was investigated and is shown in Figure 3b–d. The cyclic tests were conducted in a similar potential range for 50 cycles. The capacity of the cell (Zn, $LiBH_4$, and $AB/LiBH_4/Li$) was found to be increased to 574 $mAhg^{-1}$ after 50 cycles in comparison to the initial capacity of 506 $mAhg^{-1}$. This increase in capacity might be due to the contribution from carbon (AB) or might be caused due to the gradual kinetic activation of the initial material during cycling. On the other hand, in the case of $LiBH_4.LiI$, the cyclic capacity was found to increase up to 18 cycles and then decayed continuously. The high capacity might be due to the high conductivity of $LiBH_4$-LiI. However, at the same time, it also caused some unidentified side reactions (that might be the actual reason for enhanced capacity), which being irreversible in nature, caused a gradual decrease in the capacity after a few cycles. The detailed mechanism for this speculated reaction needs to be identified in the future. From the cycling results and the results at different temperatures, it was concluded that the use of $LiBH_4.LiI$ in the electrolyte layer enhanced the capacity and was capable of work even at lower temperatures. However, the cyclic behavior of this cell was not that promising and needed further engineering.
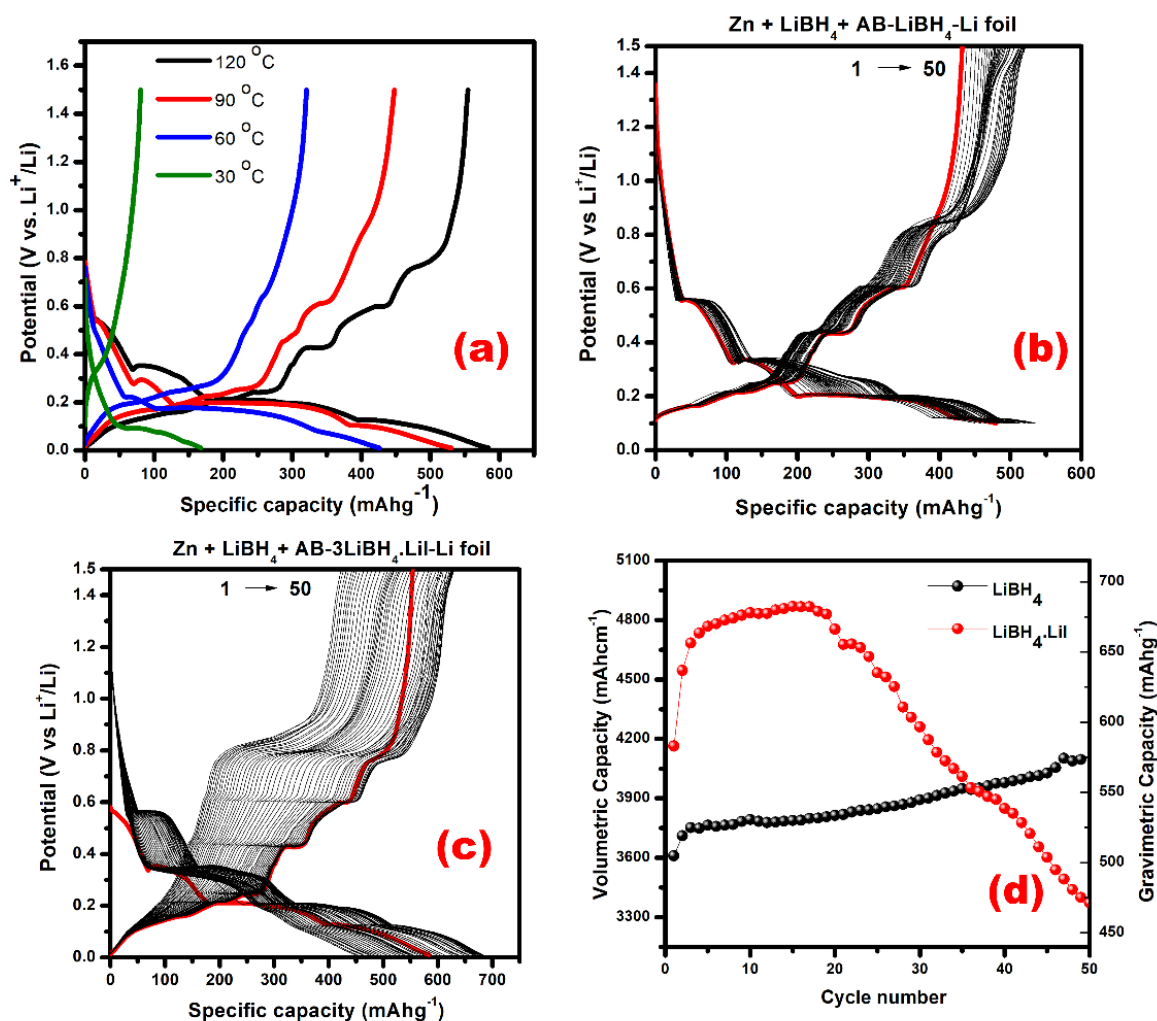
Figure 3. (**a**) Galvanostatic discharge–charge profiles for Zn-LiBH$_4$-AB/3LiBH$_4$.LiI/Li foil coin cell at different temperatures; (**b**) cycling performance of Zn-LiBH$_4$-AB/LiBH$_4$/Li foil up to 50 cycles; (**c**) cycling performance of Zn-LiBH$_4$-AB/LiBH$_4$.LiI/Li foil up to 50 cycles; (**d**) comparison of cyclic stability of composite using two different electrolytes in terms of volumetric capacity vs. cycle number.

3. Materials and Methods

Electrode and Electrolyte Preparation: Zinc (Zn) metal was purchased from Kojundo Chemical Laboratory Co., Ltd. (SAKADO, Japan), Japan, of 99.99% purity. The implementation of the purchased metal was performed without any further treatment. The electrolyte used in the present studies was LiBH$_4$, which was purchased from Sigma Aldrich (Tokyo, Japan) of purity >95%. The LiBH$_4$ was heated at 200 °C for 24 h in a vacuum to ensure that no moisture or impurity was left in the LiBH$_4$. For the second electrolyte, i.e., LiBH$_4$.LiI, heated LiBH$_4$ and as-received LiI was milled for 20 h following a 30 min rest pattern after each hour of milling using planetary type (Fritsch P7). A total of 20 SUJ balls were used in a 30 mL milling pot for 1 g of sample. The acetylene black (AB) was dried at similar conditions to those of the LiBH$_4$. The composite electrode was prepared in a weight ratio of Zn: LiBH$_4$: AB of 40:30:30 by high-energy ball milling for 2 h using a 30 min rest pattern after 1 h of milling.

Characterization: Structural properties of the prepared anode and the phase changes during electrochemical charging and discharging were measured by X-ray diffraction (XRD) studies using a Rigaku RINT 2500 diffractometer equipped with CuKα radiation. The voltage and current associated with XRD were 40 kV and 200 mA, respectively. All the

XRD measurements were conducted without the exposure of samples to air by covering them using a polyimide sheet (Dupont-Toray Co., Ltd., Kapton, Japan) and vacuum grease.

Cell fabrication and electrochemical measurements: All of the cell fabrication process was conducted in an Ar-filled glove box. For the coin cell preparation, the composite (zinc, $LiBH_4$, and AB) was used as one electrode, and Li foil was used as another electrode. A thick layer of electrolytes ($LiBH_4$ and $LiBH_4$-LiI) was sandwiched between both electrodes. The layered combinations of both arrangements are shown in Figure 4. In the beginning, the Li foil and the electrolyte were pressed under 10 MPa for 5 min. Then, the composite material was uniformly spread on the surface of the electrolyte, which was again pressed under 40 MPa for 5 min. This trilayer pellet was sealed using a 2032 coin-cell-type holder. The complete arrangement of the cell can be clearly understood by the schematic diagram in Figure 4. To understand the reaction potentials of the prepared cells, the cyclic voltammetry measurements were performed in the potential range of 0.1–1.5 V at 0.1 mV/s. The electrochemical impedance spectroscopy (EIS) measurements were carried over the frequency range of 10 mHz to 100 kHz using a Biologic SAS (SP-150) system. The electrochemical performances of the prepared cells were recorded with an automatic battery-testing system (Hokuto Denko Charge/Discharge Unit HJ-SD8) in the potential range of 0.01–1.5 V at different current rates and temperatures.
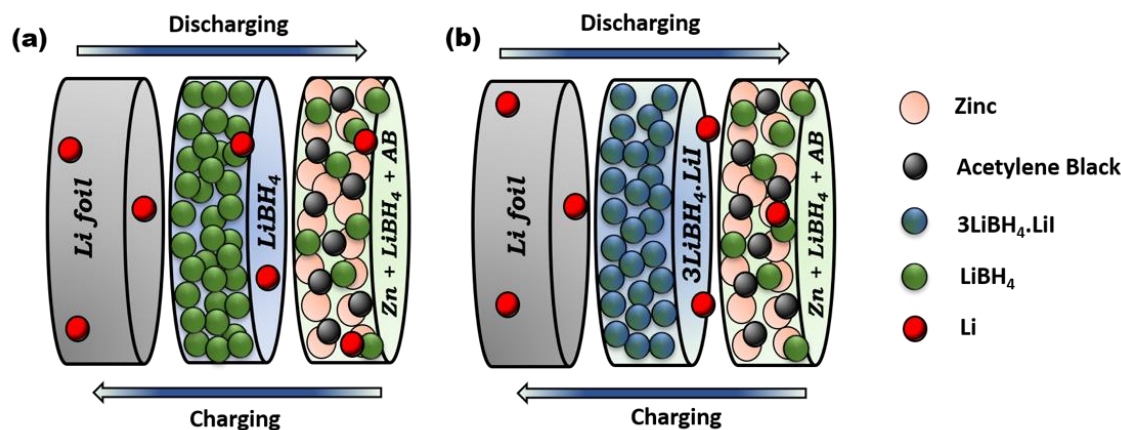

Figure 4. Battery assembly using both electrolyte layers: (**a**) Zn, $LiBH_4$, and AB using $LiBH_4$ electrolytes; and (**b**) Zn, $LiBH_4$, and AB using $3LiBH_4$.LiI electrolytes.

4. Conclusions

In conclusion, the implementation of a zinc-metal-based anode was tested for all-solid-state lithium-ion batteries. A detailed electrochemical mechanism for the $LiBH_4$ electrolyte was established. The electrochemical cycling was tested with two different combinations, i.e., Zn, $LiBH_4$, and carbon with $LiBH_4$ or $LIBH_4$.LiI. The gravimetric capacity was found as 507 mAhg^{-1} for the cell having $LiBH_4$ in the anode and the electrolyte layer, which corresponded to the volumetric capacity at 3596 mAhcm^{-3} that made this anode material suitable for applications with the requirement of small space. The capacity was found to be increased further with cycling due to kinetic activation. It was also concluded that the cell also worked at room temperature when the $LiBH_4$ electrolyte layer was replaced by an $LiBH_4$.LiI electrolyte. Further tuning of the electrolyte and anode combination is needed for the improvement of cycling at room temperature.

References

1. Dincer, I. Renewable energy and sustainable development: A crucial review. *Renew. Sustain. Energy Rev.* **2000**, *4*, 157–175. [CrossRef]
2. Gross, R.; Leach, M.; Bauen, A. Progress in renewable energy. *Environ. Int.* **2003**, *29*, 105–122. [CrossRef]
3. Lund, H. Renewable energy strategies for sustainable development. *Energy* **2007**, *32*, 912–919. [CrossRef]
4. Bull, S.R. Renewable energy today and tomorrow. *Proc. IEEE* **2001**, *89*, 1216–1226. [CrossRef]
5. Harjanne, A.; Korhonen, J.M. Abandoning the concept of renewable energy. *Energy Policy* **2019**, *127*, 330–340. [CrossRef]
6. Doughty, D.H.; Roth, E.P. A general discussion of Li ion battery safety. *Electrochem. Soc. Interface* **2012**, *21*, 37.
7. Edstroem, K.; Gustafsson, T.; Thomas, J.O. The cathode–electrolyte interface in the Li-ion battery. *Electrochim. Acta* **2004**, *50*, 397–403. [CrossRef]
8. Goodenough, J.B.; Gao, H. A perspective on the Li-ion battery. *Sci. China Chem.* **2019**, *62*, 1555–1556. [CrossRef]
9. Chombo, P.V.; Laoonual, Y. A review of safety strategies of a Li-ion battery. *J. Power Sources* **2020**, *478*, 228649. [CrossRef]
10. Nitta, N.; Wu, F.; Lee, J.T.; Yushin, G. Li-ion battery materials: Present and future. *Mater. Today* **2015**, *18*, 252–264. [CrossRef]
11. Luntz, A.C.; Voss, J.; Reuter, K. Interfacial challenges in solid-state Li ion batteries. *J. Phys. Chem. Lett.* **2015**, *6*, 4599–4604. [CrossRef]
12. Danilov, D.; Niessen, R.A.H.; Notten, P.H.L. Modeling all-solid-state Li-ion batteries. *J. Electrochem. Soc.* **2010**, *158*, A215. [CrossRef]
13. Kim, D.H.; Oh, D.Y.; Park, K.H.; Choi, Y.E.; Nam, Y.J.; Lee, H.A.; Lee, S.-M.; Jung, Y.S. Infiltration of solution-processable solid electrolytes into conventional Li-ion-battery electrodes for all-solid-state Li-ion batteries. *Nano Lett.* **2017**, *17*, 3013–3020. [CrossRef] [PubMed]
14. Du, M.; Liao, K.; Lu, Q.; Shao, Z. Recent advances in the interface engineering of solid-state Li-ion batteries with artificial buffer layers: Challenges, materials, construction, and characterization. *Energy Environ. Sci.* **2019**, *2*, 1780–1804. [CrossRef]
15. Van Den Broek, J.; Afyon, S.; Rupp, J.L.M. Interface-engineered all-solid-state Li-ion batteries based on garnet-type fast Li$^+$ conductors. *Adv. Energy Mater.* **2016**, *6*, 1600736. [CrossRef]
16. Manthiram, A.; Yu, X.; Wang, S. Lithium battery chemistries enabled by solid-state electrolytes. *Nat. Rev. Mater.* **2017**, *2*, 1–16. [CrossRef]
17. Wang, C.; Fu, K.; Kammampata, S.P.; McOwen, D.W.; Samson, A.J.; Zhang, L.; Hitz, G.T.; Nolan, A.M.; Wachsman, E.D.; Mo, Y.; et al. Garnet-type solid-state electrolytes: Materials, interfaces, and batteries. *Chem. Rev.* **2020**, *120*, 4257–4300. [CrossRef]
18. Raj, R.; Wolfenstine, J. Current limit diagrams for dendrite formation in solid-state electrolytes for Li-ion batteries. *J. Power Sources* **2017**, *343*, 119–126. [CrossRef]
19. Tong, Z.; Wang, S.-B.; Liao, Y.-K.; Hu, S.-F.; Liu, R.-S. Interface between solid-state electrolytes and Li-metal anodes: Issues, materials, and processing routes. *ACS Appl. Mater. Interfaces* **2020**, *12*, 47181–47196. [CrossRef]
20. Zhang, Q.; Cao, D.; Ma, Y.; Natan., A.; Aurora, P.; Zhu, H. Sulfide-Based Solid-State Electrolytes: Synthesis, Stability, and Potential for All-Solid-State Batteries. *Adv. Mater.* **2019**, *31*, 1901131. [CrossRef]
21. Liu, D.; Zhu, W.; Feng, Z.; Guerfi, A.; Vijh, A.; Zaghib, K. Recent progress in sulfide-based solid electrolytes for Li-ion batteries. *Mater. Sci. Eng. B* **2016**, *213*, 169–176. [CrossRef]
22. Takada, K.; Inada, T.; Kajiyama, A.; Kouguchi, M.; Sasaki, H.; Kondo, S.; Michiue, Y.; Nakano, S.; Tabuchi, M.; Watanabe, M. Solid state batteries with sulfide-based solid electrolytes. *Solid State Ion.* **2004**, *172*, 25–30. [CrossRef]
23. El Kharbachi, A.; Sørby, M.H.; Nygård, M.M.; Hauback, B.C. Borohydride-based Solid-state Electrolytes for Lithium Batteries. In Proceedings of the IEEE 2019 7th International Renewable and Sustainable Energy Conference (IRSEC), Agadir, Morocco, 27–30 November 2019; pp. 1–4.
24. Zhang, T.; He, W.; Zhang, W.; Wang, T.; Li, P.; Sun, Z.; Yu, X. Designing composite solid-state electrolytes for high performance lithium ion or lithium metal batteries. *Chem. Sci.* **2020**, *11*, 8686–8707. [CrossRef]
25. Zhao, C.; Liang, J.; Li, X.; Holmes, N.; Wang, C.; Wang, J.; Zhao, F.; Li, S.; Sun, Q.; Yang, X.; et al. Halide-based solid-state electrolyte as an interfacial modifier for high performance solid-state Li–O$_2$ batteries. *Nano Energy* **2020**, *75*, 105036. [CrossRef]

26. Park, K.-H.; Kaup, K.; Assoud, A.; Zhang, Q.; Wu, X.; Nazar, L.F. High-voltage superionic halide solid electrolytes for all-solid-state Li-ion batteries. *ACS Energy Lett.* **2020**, *5*, 533–539. [CrossRef]

27. Li, X.; Liang, J.; Yang, X.; Adair, K.R.; Wang, C.; Zhao, F.; Sun, X. Progress and perspectives on halide lithium conductors for all-solid-state lithium batteries. *Energy Environ. Sci.* **2020**, *13*, 1429–1461. [CrossRef]

28. Kisu, K.; Kim, S.; Oguchi, H.; Toyama, N.; Orimo, S. Interfacial stability between LiBH$_4$-based complex hydride solid electrolytes and Li metal anode for all-solid-state Li batteries. *J. Power Sources* **2019**, *436*, 226821. [CrossRef]

29. Unemoto, A.; Yasaku, S.; Nogami, G.; Tazawa, M.; Taniguchi, M.; Matsuo, M.; Ikeshoji, T.; Orimo, S.-I. Development of bulk-type all-solid-state lithium-sulfur battery using LiBH$_4$ electrolyte. *Appl. Phys. Lett.* **2014**, *105*, 83901. [CrossRef]

30. Takahashi, K.; Hattori, K.; Yamazaki, T.; Takada, K.; Matsuo, M.; Orimo, S.; Maekawa, H.; Takamura, H. All-solid-state lithium battery with LiBH4 solid electrolyte. *J. Power Sources* **2013**, *226*, 61–64. [CrossRef]

31. Sharma, K.; Singh, R.; Tripathi, B.; Ichikawa, T.; Kumar, M.; Jain, A. All-Solid-State Li-Ion Batteries Using a Combination of Sb$_2$S$_3$/Li$_2$S-P$_2$S$_5$/Acetylene Black as the Electrode Composite and LiBH4 as the Electrolyte. *ACS Appl. Energy Mater.* **2021**, *4*, 6269–6276. [CrossRef]

32. Kumari, P.; Awasthi, K.; Agarwal, S.; Ichikawa, T.; Kumar, M.; Jain, A. Flower-like Bi$_2$S$_3$ nanostructures as highly efficient anodes for all-solid-state lithium-ion batteries. *RSC Adv.* **2019**, *9*, 29549–29555. [CrossRef] [PubMed]

33. El Kharbachi, A.; Uesato, H.; Kawai, H.; Wenner, S.; Miyaoka, H.; Sørby, M.H.; Fjellvåg, H.; Ichikawa, T.; Hauback, B.C. Hauback MgH$_2$–CoO: A conversion-type composite electrode for LiBH$_4$-based all-solid-state lithium ion batteries. *RSC Adv.* **2018**, *8*, 23468–23474. [CrossRef] [PubMed]

34. Cano-Banda, F.; Gallardo-Gutierrez, A.; Luviano-Ortiz, L.; Hernandez-Guerrero, A.; Jain, A.; Ichikawa, T. High capacity MgH2 composite electrodes for all-solid-state Li-ion battery operating at ambient temperature. *Int. J. Hydrogen Energy* **2021**, *46*, 1030–1037. [CrossRef]

35. Maekawa, H.; Matsuo, M.; Takamura, H.; Ando, M.; Noda, Y.; Karahashi, T.; Orimo, S.-I. Halide-stabilized LiBH$_4$, a room-temperature lithium fast-ion conductor. *J. Am. Chem. Soc.* **2009**, *131*, 894–895. [CrossRef] [PubMed]

36. Ryu, J.; Hong, D.; Lee, H.-W.; Park, S. Practical considerations of Si-based anodes for lithium-ion battery applications. *Nano Res.* **2017**, *10*, 3970–4002. [CrossRef]

37. Kumari, P.; Sharma, K.; Pal, P.; Kumar, M.; Ichikawa, T.; Jain, A. Highly efficient & stable Bi & Sb anodes using lithium borohydride as solid electrolyte in Li-ion batteries. *RSC Adv.* **2019**, *9*, 13077–13081. [PubMed]

38. Tian, H.; Xin, F.; Wang, X.; He, W.; Han, W. High capacity group-IV elements (Si, Ge, Sn) based anodes for lithium-ion batteries. *J. Mater.* **2015**, *1*, 153–169. [CrossRef]

39. Hwa, Y.; Sung, J.H.; Wang, B.; Park, C.-M.; Sohn, H.-J. Nanostructured Zn-based composite anodes for rechargeable Li-ion batteries. *J. Mater. Chem.* **2012**, *22*, 12767–12773. [CrossRef]

40. Kumari, P.; Singh, R.; Awasthi, K.; Ichikawa, T.; Jain, A.; Kumar, M. Electrochemical reaction mechanism for Bi$_2$Te$_3$-based anode material in highly durable all solid-state lithium-ion batteries. *J. Mater. Sci. Mater. Electron.* **2020**, *31*, 16429–16436. [CrossRef]

41. Kumari, P.; Singh, R.; Awasthi, K.; Ichikawa, T.; Kumar, M.; Jain, A. Highly stable nanostructured Bi$_2$Se$_3$ anode material for all solid-state lithium-ion batteries. *J. Alloys Compd.* **2020**, *838*, 155403. [CrossRef]

42. Kumari, P.; Pal, P.; Shinzato, K.; Awasthi, K.; Ichikawa, T.; Jain, A.; Kumar, M. Nanostructured Bi$_2$Te$_3$ as anode material as well as a destabilizing agent for LiBH$_4$. *Int. J. Hydrogen Energy* **2019**, *45*, 16992–16999. [CrossRef]